Defense Technical Information Center Compilation Part Notice

ADP023843

TITLE: Time Accurate Unsteady Simulation of the Stall Inception Process in the Compression System of a US Army Helicopter Gas Turbine Engine

DISTRIBUTION: Approved for public release, distribution unlimited

This paper is part of the following report:

TITLE: Proceedings of the HPCMP Users Group Conference 2004. DoD High Performance Computing Modernization Program [HPCMP] held in Williamsburg, Virginia on 7-11 June 2004

To order the complete compilation report, use: ADA492363

The component part is provided here to allow users access to individually authored sections of proceedings, annals, symposia, etc. However, the component should be considered within the context of the overall compilation report and not as a stand-alone technical report.

The following component part numbers comprise the compilation report:
ADP023820 thru ADP023869

Time Accurate Unsteady Simulation of the Stall Inception Process in the Compression System of a US Army Helicopter Gas Turbine Engine

Michael D. Hathaway and Greg Herrick
US Army Research Laboratory (ARL),
Vehicle Technology Directorate,
Aberdeen Proving Ground, MD
{mhathaway,
Gregory.P.Herrick}@grc.nasa.gov

Jenping Chen
Mississippi State University,
Mississippi State, MS
chen@ERC.MsState.Edu

Robert Webster
University of Tennessee,
Memphis, TN
Robert-Webster@utc.edu

Abstract

The operational envelope of gas turbine engines such as those employed in the Army Blackhawk helicopter is constrained by the stability limit of the compression system. Technologies developed to improve the stable operating range of gas turbine compressors lack a fundamental understanding beneficial to design guidance. Improved understanding of the stall inception process and how stall control technologies mitigate such will provide compressors with increased tolerance to stall, thereby expanding the operational envelope of military gas turbine engines.

Compressors which consist of multiple stages of stationary and rotating blade rows can include shocks, vortices, separations, secondary flows, shock/boundary layer interactions, and turbulent wakes, all of which grow in severity as a compressor approaches stall. As a compressor nears stall the flow field is no longer periodic from passage to passage so all blade passages must be computed. For a typical multistage compressor this becomes a formidable computational challenge requiring access to massively parallel machines in order to meet the computational and memory demands of the problem.

We are using a time-accurate CFD code to simulate the unsteady stall inception process, both with and without stall control technology, in the compression system of the T700 engine which is employed in the Army Blackhawk Helicopter. This work will provide the first-ever 3-dimensional viscous time-accurate simulation of the stall inception process in a multistage compressor, providing insight into the causal link between compressor blade design parameters and the stable operating limit, which will be used to guide new design practices leading to compressor designs with increased tolerance to stall.

This paper presents progress to date on this DoD Challenge Project.

Introduction

Gas turbine engines are the prime movers in a large number of combat vehicles for the Army, Navy, and Air Force including surface ships, tanks, manned and unmanned fixed-wing and rotary-wing combat aircraft, and logistic aircraft. These engines must perform reliably in harsh operating arenas while maintaining a high degree of operational availability. The stable operating envelope of gas turbine engines is dictated in large part by the aerodynamic stability (tolerance to stall) of the engine compression system.

Factors that reduce compression system tolerance to stall are eroding due to ingestion of debris during takeoff and landing from damaged and unimproved fields and during low-altitude maneuvers, distorted intake flows during combat maneuvers, and ingestion of hot gas during munitions firing. In addition, the increased use of stealth technology is generating requirements that conceal engine intakes and exhaust streams from direct observation, further reducing intake flow quality and thus degrading compressor stability.

Researchers at the ARL Vehicle Technology Directorate and NASA Glenn Research Center have developed compressor stall control technologies that have been successfully demonstrated in compressor component tests[1-6]. These stability enhancement technologies have been developed through parametric experimental studies. Their effectiveness is based on altering the unsteady flow field near the compressor blade tips[1-6]. However, there is a lack of fundamental understanding of the fluid mechanic processes of stall inception and how these stall control technologies mitigate stall to achieve increased

compressor stability. Improved understanding of the stall inception process will guide the further development of stall control devices and of compressor blading with increased tolerance to stall, thereby expanding the operational envelope of military gas turbine engines.

During the last ten years steady-flow computational simulations have provided an increasingly accurate prediction of the flow up to the point of compressor stall. However, attempts to study stall through unsteady simulations of a subset of the blades in a compressor blade row[7] or through reduced-order unsteady flow models[9] have been unsuccessful to date. Since the temporal flow field variations that occur during stall inception are not harmonics of blade passing frequency, the unsteady flow in each blade passage within a blade row must be simulated in order to study the transition from a steady flow state into the unsteady stalled flow state. Such simulations have been done two-dimensionally[8], but stall is an inherently three-dimensional unsteady phenomena[8]. We have realized major improvements in the ability to accurately simulate *steady* flows near the blade tip in axial compressor rotors through improved gridding techniques[10] and have concurrently improved the accuracy of an *unsteady* flow solver for turbomachinery blading (TURBO) through improvements in grid generation and turbulence modeling[11].

The TURBO code is fully parallelized and has been successfully used as a production code for unsteady simulations of near design point conditions of multistage compressors. The present effort utilizes the time-accurate CFD code TURBO to simulate the unsteady stall inception process, both with and without stall control technology, in the compression system of an Army gas turbine engine. This exercise will provide the first-ever 3D viscous full-annulus unsteady simulation of the stall inception process, providing insight into the causal link between compressor blade design parameters and the stable operating limit.

This will be a significant contribution to the Army/DoD community which utilizes gas turbines in a large number of combat vehicles (Comanche, Apache, Black Hawk, M1, FCS, manned and unmanned fixed and rotary-wing aviation platforms) that typically must operate under the most severe conditions. The benefits of improved understanding of the stall inception process will yield compressor designs that are able to operate closer to their maximum efficiency operating point while still providing adequate stall margin. *This would yield a significant reduction in logistics support due to the considerable fuel savings that could be achieved resulting in substantial enhancement of force mobility, survivability, and sustainability.*

2. Problem and Methodology

Stall detection schemes and stall controllers rely on the presence of small-amplitude stall precursive disturbances (which are measured with high-response transducers and form the inputs to stall warning and stall control systems). The uncontrolled growth of these disturbances leads to stall. We do not currently understand the causal link between these disturbances and the fluid mechanic processes occurring within the compressor blade row just prior to stall. Furthermore we don't understand the fundamental fluid mechanics of how stall control technology extends the stable operating range of a compressor. Determining this causal link and how stall control technology beneficially affects such to extend the stable operating range of a compressor are the key objectives of this effort.

Typical flow phenomena involved in rotating machinery can include shocks, vortices, separations, secondary flows, shock and boundary layer interactions, and turbulent wakes. Any CFD simulation of turbomachinery must be capable of resolving the multiple length and time scales found in these flows. A consistent research effort toward the development of such a CFD code has been underway for some time at Mississippi State University. The TURBO code, whose development has been supported by NASA, DOD, and industry, is a flow solver that approaches the goal of a high fidelity simulation of multistage turbomachinery flow physics[11].

The TURBO code was developed to simulate the highly complex flow fields generated by rotating machinery. This code is a finite volume, implicit scheme for unsteady, 3-D, compressible, viscous flows. It solves the Reynolds averaged Navier-Stokes equations. Flux vector splitting is used in evaluating flux Jacobians on the left hand side while Roe's flux difference splitting is used to form a higher-order TVD scheme for the evaluation of convective fluxes on the right hand side. Newton sub-iterations are applied to obtain a converged solution within one time step. Numerical instability problems can occur as the grids are clustered on the walls in order to resolve the viscous effects. Therefore, a modified two-pass scheme similar to Gauss-Seidel is used to reduce the errors brought about by the approximate factorization of the old two-pass scheme, and hence allows larger CFL numbers for the Navier Stokes type grids.

For implicit schemes, flux jacobians are needed to linearize the physical flux vectors, which contain both inviscid and viscous components. The viscous jacobians were done with a numerical formulation in the older versions of the code. Redundant computation of viscous fluxes had consumed almost one third of the entire computing time. To improve the performance, an analytical formulation was implemented. The result is a

30% reduction in CPU time and enhanced code robustness.

The steady Navier-Stokes Turbomachinery solver APNASA[12] is used to compute an initial guess at the time-accurate flow field for the TURBO code. Starting the TURBO computation from this high quality initial flow field makes it easier to overcome the initial transient phase during the computation and in some cases results in an order of magnitude reduction in the CPU time that is required to reach a converged time-accurate solution[13]. This procedure is well demonstrated and is the standard method for beginning a time accurate calculation.

Both TURBO and APNASA use an advanced two-equation turbulence model that was developed specifically for turbomachinery flows by ICOMP at NASA Glenn Research Center[14]. This model has demonstrated superior ability to accurately simulate important viscous effects, such as shock/boundary layer interaction in turbomachinery environments.

APNASA is a fully operational production code that is in common use by most US engine manufacturers. There is a large experience base at NASA Glenn for the setup and execution of simulations using APNASA. The code is well validated for the compressor geometries that are the focus of the unsteady computations presented herein.

The TURBO code is also a fully operational production code that has been released to industry. There is an experience base at NASA Glenn Research Center in the use of this code for turbomachinery geometries. TURBO has been validated with single and multi-blade row turbomachinery cases. An isolated rotor (one blade row), and a compressor stage (two blade rows) cases have been run on the DoD Naval Oceanographic Office MSRC Cray T90 machine. A multistage compressor (5 blade rows) case has been run on the DoD Naval Oceanographic Office MSRC Origin machine. Resource estimates for this project are based on scaling these cases to full-annulus multistage simulations.

Computational issues that arise for this Challenge project include both portability and scalability of the flow solvers, as well as the spatial resolution and time steps needed for accurate simulations of stall characteristics. The parallel TURBO code is implemented in a portable, scalable form for distributed-memory parallel computers using MPI message passing[15]. The solution algorithm is an iterative implicit time-accurate scheme with characteristics-based finite-volume spatial discretization. The Newton sub-iterations are solved using a concurrent block-Jacobi symmetric Gauss-Seidel (BJ-SGS) relaxation scheme. Unsteady blade-row interaction is treated either by simulating full or periodic sectors of blade-rows, or by solving within a single passage for each row using phase-lag and wake-blade interaction approximations at boundaries. A scalable dynamic sliding-interface algorithm is used here, with an efficient parallel data communication between blade rows in relative motion.

The parallel code is implemented by a single-program multiple-data (SPMD) parallelization strategy. In this strategy, a single program is replicated for each processor and run with the data associated with a subdomain of the original computational domain. The parallel communication framework has been coded to support the solution of problems using multi-block structured grids in which the block connectivity of the grid blocks is arbitrary. The original grids, one per blade passage, need to be partitioned before the execution of the flow solver. The grid partitioning is done with the preprocessor GUMBO[16], which features a graphical user interface. The approach to parallelization for large-scale complex problems is discussed in further detail in References 17–19. Portability has been demonstrated for numerous parallel platforms including Cray T3E, IBM SP-2, Sun Enterprise ULTRA 10000, SGI Origin 2000, and PCA Arrays, as well as workstation clusters. The parallel TURBO code to be used is an evolution of the sequential version that has been validated very extensively over the past ten years. The parallel version has been validated by repeating selected flow cases previously validated using the sequential version.

To facilitate and expedite setup of a full-annulus simulation, the domain decomposition preprocessor GUMBO was modified so that the entire setup process can be done automatically. This process includes rotate-copying the grid and solution into a full-annulus, partitioning and renumbering of the blocks, generating all boundary conditions, and connectivity information. This improvement is significant in that it reduces the setup time for cases of this kind from days to hours.

2.1. Computing Resources.

Hardware improvement is a major factor in achieving fast turnaround. The computers used in this study ranged from 800 MHz Pentium II processors for Linux clusters to 1.3 GHz Power 4 processors for the IBM P4 supercomputer. The scalable parallel architecture of TURBO is able to utilize these improved hardware capabilities as they become available. The parallel solutions typically have communications overhead of only 10–15%. Scalability studies performed last year indicated linear or even super linear speedups were achievable as long as parallel efficiency maintained at 85% or above, with the parallel efficiency as a function of load balance and network capacity. On average the parallel efficiency for all the axial compressor simulations on the IBM's is above 90%. It is therefore assured that the calculations on these computers are highly scalable.

The IBM SP3/4 systems were used for all simulations conducted in this study. Table 1 shows the computer usage for Stage 35 with injection. Timings are for the SP4, which are the CPU hours needed to converge a stable case (away from stall). Even though more processors (CPUs) are needed for the half or full-annulus simulations, the convergence speed is one order of magnitude faster than the phase-lag simulations. The overall resource requirements can be expressed in total CPU-hrs used for the simulation (number of processors multiplied by time used). The full-annulus simulation seemed to provide the best return on investment as it produces the highest fidelity (least assumptions) result with only a small increase in total CPU-hrs.

Table 1. Computer usages for Stage35 simulations with tip injection

	Passages	CPU	Converge time (hrs.)	CPU-hrs
Phase-lag	3	34	100 (10 rev)	3400
Half-annulus	47	164	24 (1 rev)	3936
Full-annulus	94	328	24 (1 rev)	7872

Results

The overall objective of this effort is to predict and characterize the stall inception and control process in the compression system of the T700 engine used in the US Army Blackhawk helicopter. The T700 engine includes both a high speed multistage axial and a centrifugal compressor stage. The capability of the TURBO code to simulate the flow fields in both high speed axial and centrifugal compressors as well as to predict stall range extension will be assessed by comparing experimental measurements obtained both with and without stall control technology in both a high speed axial compressor, Stage 35, and a high speed centrifugal compressor, CC3. The results presented herein reflect progress to date.

The time accurate simulations of both a high speed single stage axial, Stage 35[1-5,20], (Figure 1) and a high speed centrifugal compressor, CC3[6,21], (Figure 2) for which detailed experimental data are available provide assessment of the capability of the TURBO code for predicting the stall inception processes in a multistage axi-centrifugal compressor (see Figure 3) as employed in the Army Blackhawk helicopter.

3.1. Stage 35.

The high-speed single-stage axial compressor, Stage 35, operating at 17189 RPM at design speed conditions (20.2 kg/sec) produces 1.82 total pressure ratio.

This axial compressor consists of 36 rotor blades followed by 46 stator blades.

To facilitate comparison of simulations with and without tip injection, the simulations of stage 35 used a three-blade-row grid as shown in Figure 4. This grid consists of an injector (blue), a rotor (pink), and a stator (green) blade row. The injector has twelve injectors that are equidistant in the circumferential direction and each of these injectors is treated as a 'blade passage'. The injector grid is followed by the rotor grid, and then the stator grid. The effect of injection is modeled through addition of source terms in the injector grid. For the no-injection simulations the injection can be turned off by removing the source terms. A similar grid model approach was used for the CC3 centrifugal compressor simulations with the exception that the injection model did not require an additional block as it was introduced as an injection boundary condition in the outer case flow path.

3.1.1. Stage 35 without Injection

This case was conducted to investigate the unsteady flow development of stall inception without stall control. During the stall inception process, stall cells can rotate around the annulus and the assumption of both spatial and temporal periodicity is not valid. The only correct modeling technique is to compute the full-annulus of the compression system. However, before stall occurs, the flow can be reasonably modeled as an axi-symmetric flow. Half-annulus simulations with spatial periodicity were first conducted to save computer resources.

Compressor characteristics (speed lines) were generated by incrementally increasing the exit static pressure. A comparison of the TURBO predictions using half-annulus conditions to the experimentally measured design speed lines for Stage 35 is shown in Figure 5. The solid casing (no injection) case compares reasonably, with TURBO predicting higher pressure rise. As the flow started to show asymmetric features, which occurs after raising the backpressure by 0.1% to restart from the last stable operating point (the left-most open circle) of the solid casing case, the simulation was switched to full-annulus to record the stall inception process. These calculations used 164 CPUs for the half-annulus and 328 CPUs for the full-annulus. This is probably a first of its kind simulation in modeling the stall inception process in a high speed transonic compressor stage with a full-annulus grid. In the stall inception simulation, four numerical probes were set up to record the unsteady axial velocity variation as shown in Figure 6. The probes were located 10% chord downstream of the rotor trailing edge at 98% span. They are spaced 90 degrees apart and fixed in the absolute coordinate frame of reference. For the stable operating conditions away from stall inception, due

to the weaker stator potential field, the flows between rotor passages are relatively similar. The unsteady variations at the probe locations are dominated by the rotor passing frequency. This can be observed in Figure 6 before iteration 6000. As the stall cells begin to develop, the magnitude of the oscillations increases and the flow field becomes asymmetric. The axial velocity variations start to show frequencies other than the rotor passing as seen in the velocity traces after iteration 6000. The additional frequencies are related to the unsteady development of the rotor tip clearance flows and local separations within rotor passages during the stall inception process.

The development of stall inception characteristics can be seen in the axial velocity (Figure 7) and entropy contours (Figure 8). The two snapshots are taken at iterations 6401 and 7901, which are about a half of a rotor revolution (1800 iterations) apart, and correspond to mass flows at 18.19 kg/s and 18.08 kg/s respectively. Iteration 7901 represents the condition deeper into stall. The low momentum (green color) regions indicating blockage within the passage grow as the flow enters deeper into stall. This can be seen more so in the stator passages. In the entropy contours, high entropy regions (red color) near the suction surface begin to grow and spread to encompass more rotor passages as the flow progresses more into stall. This indicates the flow is becoming more chaotic on the suction surfaces. As the simulation continued the blockage increased even more as was demonstrated by a rapid decrease in mass flow rate (not shown here). Reversed flow finally developed in the middle of the rotor blade passages, which led to termination of the simulation.

The development of the asymmetric flow field may be an indication of the onset of a rotating stall. The simulation stopped before these reversed flows had a chance to develop into a more periodic rotating pattern. Efforts to examine the growth rate and pattern of the reversed flow before the simulation stopped are underway to find out if it resembles any type of stall inception process.

3.1.2. Stage 35 with Injection

One of the main topics addressed in the present investigation is the use of mass injection upstream of the rotor tip to increase the range of the compressor mass flow rates for which stable operation is possible. The injected flow is modeled by the addition of source terms equivalent to injection of 5.9% design mass flow (20.34 kg/s) or 1.2 kg/s downstream of the axial direction and with no yaw.

This case was first conducted with the phase-lag modeling technique where only one blade passage is needed for each of the three blade rows. However, the

inability of phase-lag modeling in capturing the spatial periodicity between the injector and stator resulted in a discrepancy of mass flow of 0.5 kg/sec between the rotor and stator. Because of the strong impact of the high-speed injected flow (as compared to a wake influence) it was decided that in order to obtain mass conservation throughout all blade rows it was necessary to model the true periodicity, which can only be achieved with at least a half-annulus simulation with the blade count of 6-18-23.

TURBO prediction of the steady injection using half-annulus conditions is compared to the experimental measurement as shown in Figure 5. Similar to the no-injection case, the overall performance compares reasonably, with TURBO predicting a higher pressure rise. There is no predicted range extension with the stall control technology. The discrepancy in predicting range extension from the measurements is being investigated. And some speculations arose from the following analysis.

Axial velocity and entropy contours near the casing are shown in Figure 9. The injected flows are seen as the high axial velocity and low entropy areas ahead of the rotor. The contour plots are the instantaneous images taken from the last operating point of the injection speed line in Figure 6. This operating point has the same level of mass flow as that examined in the previous no-injection case. The point is very close to the boundary of the operating range that, without stall control, will develop into an unstable stall condition. As shown in Figure 10, pockets of low momentum flow appear near the suction surface of the rotor blades as the rotor passages move out of the influence of the injected flow. As the rotor passage enters the region of injected flow, the pockets disappear and presumably the blade loading decreases. Equally interesting to note is that the low momentum flow pockets reappear as soon as the rotor passage moves out of the injected flow region. The fast 'kick back' of the low momentum flow contributes to large oscillations in the flow structure experienced by the leading edge of the rotor. As a result, numerical instability developed near the leading edge tip areas which eventually led to termination of the simulation. Modification of the numerical scheme so the code can better tolerate the large oscillations is underway in an effort to overcome this difficulty.

Similar behavior of entropy evolution can be observed in Figure 9, where high entropy pockets (red color) near the suction surface disappear as the rotor passages move into the injected flows and reappear as soon as the passages move out of the injected flow. Comparing to Figure 8, when the stall control is in effect, the overall entropy level is lower, and fewer high entropy pockets are found. This demonstrates that the injection can help in stabilizing the otherwise unstable flow, which without such stall control technology is prone to stall.

Figure 10 shows contours of relative total pressure on an annular section near the rotor leading edge at an instant in time. The results are from a half-annulus simulation (6-18-23 passages, respectively) where 12 of the rotor passages are shown and the 13th passage on the right hand side of the plot is included from a half-annulus simulation without injection, but near the same operating point. A shown in Figure 10 the rotor passages which are impacted by the injectors have regions of high relative total pressure (yellow to red) near the casing and the un-injected passages have low relative total pressure (shades of blue) throughout. The un-injected passages look similar to the passage from the simulation without injection. Also shown in Figure 10 are plots of relative total pressure as a function of span and pitch at, respectively, constant pitch wise or span wise locations that pass through the injected flow. For each plot the results are plotted for several different passages: from the no injection simulation (red), and passages 1 (green), 2 (blue), 3 (black), and 6 (gold) from the injection simulation. As can be seen from these plots, for passages outside the influence of the injectors the relative total pressure is low indicating increased loading, and for passages within the influence of the injectors the relative total pressure is much higher indicating decreased loading. Again, the evidence suggests that the injection should be providing increased range as has been measured in the actual tests.

3.2. Centrifugal Compressor, CC3.

The high-speed centrifugal stage, CC3, is operating at 21,789 RPM at design speed conditions (4.54 kg/sec) produces 4:1 pressure ratio. This centrifugal compressor consists of 15 main blades, 15 splitter blades for the impeller, followed by 24 diffuser vanes.

Most of the centrifugal compressor simulations for the past year have been focused on the CC3 high-speed compressor using multiple-passage configurations. Simulations have been conducted both with and without external flow injection, which is used as a means of delaying the onset of compressor stall.

3.2.1. CC3 without Injection

As with the previous simulations of the axial compressor several levels of simulation fidelity were employed before stepping up to the full-annulus simulations. Initially phase-lag boundary conditions were used which required the least amount of resources (18 processors), then third-annulus simulations which are periodic with impeller and diffuser count (105 processors), and finally full-annulus simulations (315 processors).

Most of the non-injection simulations using phase-lag boundary conditions were conducted in the previous year's work. These runs were made to obtain computational operating points at the design speed for comparison to experiment. Also, an estimate of the stall point was obtained; this estimate served as a guide (i.e., in providing an idea as to the location of the stall point) for the full-annulus, non-injection simulation. As seen in Figure 11b, this point is represented by the left-most open circle and compares reasonably well with the experimental value.

The primary purpose for the third-annulus simulations was to perform a multiple-passage investigation of the effect of externally injected flow for stall control (to be discussed at greater length in the next section). However, a couple of operating points were simulated without injection for this configuration (open circles in Figure 11(a)). These points serve to compare with experiment in the vicinity of the on-design operating point, but primarily their purpose was that of initial conditions from which to start the third-annulus injection cases. For this reason, no non-injection, third-annulus simulations were attempted in the near-stall region.

Figure 12 is a view of the flow field in the vaneless space as well as through the diffuser passages; all velocity vectors shown are at a constant-span location near the casing. The velocity vectors show relatively small variation across the diffuser channel at this span through much of the length of the channel; this appears to breakdown somewhere toward the latter part of the channel. However, there can be quite a bit of cross-channel variation in the flow speed and direction for locations away from the casing. This can be seen in two computational planes located toward the trailing edge of the diffuser vanes; these planes are colored by Mach number and show that roughly the left half (suction side) of the channel is occupied by low-speed flow (some of which is actually reverse flow). This effect may be due to the influence of recirculation zones adjacent to the trailing edges of the diffuser vanes.

Figure 12 certainly illustrates the complexity of the flow field in this machine. Within the diffuser section alone, there are quite a variety of flow effects taking place in individual channels as well as between them. And, of course, the interaction between the impeller blades and the diffuser vanes is noticeable.

3.2.2. CC3 with Injection

The first injection case to be discussed is a single-passage (i.e., phase-lag) simulation. This case was a first attempt at incorporating flow injection via a source term file that is used to model the actual injector. The source term file is generated by a separate code and models the injector by specifying mass, momentum, and energy flux

at certain grid locations. As far as the flow-solver code is concerned, the injector modeling simply serves as an additional type of boundary condition. The injection technique modeled in all cases discussed here is applied at the casing near the inlet of a diffuser passage. The injection flow rate is approximately 1.7% of the compressor's design-point flow (4.5 kg/sec), with the primary velocity component being in the "reverse tangential" direction (i.e., in the direction opposite that of the flow exiting the impeller passages). See Skoch[6] for more discussion of this injection technique.

Results from this case were both encouraging in one sense and discouraging in another. The encouragement came from the relative ease of implementation of the injector models (little trouble was experienced by the inclusion of the modeled injection into the existing flow-solver code) and the significantly lower flow rates obtained. For example, experimental results show a flow rate of about 4.2 kg/sec for the baseline non-injection configuration. A flow rate of between 3.6 and 3.9 kg/sec was obtained for this single-passage case with injection. The discouraging aspect of this simulation was that the pressure ratio for the compressor was significantly lower than the measured values. So, for the type of injection technique being modeled, this simulated operating point was not at all comparable with the experiment.

The results discussed above for the single-passage configuration with injection should not have been entirely unexpected. Expanding this case to a full-annulus configuration would be equivalent to having an injector in every diffuser passage, which does not represent the actual test setup. This could quite likely explain both the (desirably) lower flow rate and the (undesirably) lower pressure ratio for the compressor stage.

In light of the disagreement with experiment of the simulated single-passage configuration with injection, it was decided to attempt a multiple-passage simulation that should be more realistic to the actual test configuration. However, rather than go directly to a full-annulus configuration, a 1/3-annulus case was chosen.

As mentioned earlier, the primary purpose of this particular configuration was to investigate the effect of injection. This configuration, like the actual machine, allows for diffuser passages both with and without injector flows. It also allows the required number of processors to be kept at a lower value than a full-annulus case (105 versus 315), resulting in generally lower wait times in the system queue, and a reduced rate of consumption of the allocated computational hours on the MSRC computers. Also, since the number of flow passages for both the impeller and diffuser are divisible by 3, periodic boundary conditions could be used on the outer circumferential boundaries. This type of boundary condition is quite appropriate without injectors in the diffuser passages, at least for conditions away from stall.

However, this is not so true with injectors present due to the uneven distribution of injector locations around the annulus. Though not truly correct, periodic boundary conditions were used with injection in order to assess whether or not the discrepancy in mass flow between predictions and experiment was due to the modeling restrictions associated with simulating one diffuser passage.

A number of different points were simulated using the 1/3-annulus configuration. Each point compares pretty well to the experiment (again, see Figure 11(a)); the non-injected operating points (open circles) are slightly above the experimental curve, and the injected operating points (open triangles) are shown to be a little below their associated experimental curve.

With three injectors in this 1/3-annulus configuration, the total number for an equivalent full-annulus case would be nine. Since there are only eight injectors in the actual machine, the presence of this "extra" injector coupled with the incorrect use of periodic boundary conditions could account for the lower pressure ratios with injection. However, these results are in much closer agreement with the experiment than the single-passage case. The one disappointment here is that the degree of range extension (i.e., the location of stable operating points with flow rates lower than the baseline surge point) is not as great as that shown by experiment.

Figure 13 is from the same viewpoint as that of Figure 12, with the presence and effect of the injected flow being quite visible. The reverse tangential injection flow collides with the flow exiting the impeller. This seems to force flow from near the casing toward the inner portion of the channel. This effect can be seen in the nearest channel containing an injector. A computational plane near the end of the channel (also colored by Mach number) shows that the top half of the channel is a region of low-speed flow, while the bottom half has higher-speed flow (contrast this with the same channel from Figure 12). The injection also affects the incidence angle for the diffuser vanes. Most noticeable is the vane adjacent to the injector (in the direction of impeller rotation). A relatively high-speed reverse flow can be seen wrapping around the leading edge of that vane and spilling into the next channel.

Figure 14 is a view from the exit of the diffuser section. Quite a bit of channel-to-channel variation of the flow field can be seen as a result of the injectors being present. Again referring to Figure 11(a), the results of this case look to agree reasonably well with experiment, so the modeling of the injection system seems to be having the desired effect.

Figure 15 shows a full-annulus configuration that has been simulated with injectors. The presence of the injectors can be seen by the regions of low Mach number near the leading edges of certain diffuser channels. This

figure gives a good view of the effect of injection within and between the diffuser channels. Two runs were made without injection, one near the on-design point, as well as one near stall. Both are shown as the open circles in Figure 11(b).

As with the 1/3-annulus configuration, the non-injection operating points are slightly higher (in pressure ratio) than the experimental values. With injectors present, the agreement with experiment is very good. Though some range extension is shown, these results still do not show the degree of extension as that given by experiment. But, as can be seen in Figure 11, even very slight increases in pressure ratio can result in relatively significant changes in the flow rate when operating in the near-stall region. Therefore, it is a challenge to obtain a stable operating point just before the onset of compressor instability. Attempts are ongoing to see if further improvement in range extension can be achieved with the full-annulus simulations.

3.3. T700 Multistage Axial Compressor.

This Army helicopter gas turbine engine has an axial compressor containing one IGV and 5 stages. Last year, this case was run at 98% design speed with no bleeds modeled. Span wise total conditions and flow angles are prescribed at the inlet to the computational domain. At the exit a radial equilibrium boundary condition is applied with prescribed hub static pressure. To conserve computing resources while establishing the predicted speed line characteristic the simulation was initially set up using the phase-lagged approximation in which only one blade passage is computed for each blade row. This grid had 7 million points and was partitioned into 138 blocks using the GUMBO utility. The case started to run in the reduced frequency mode for 4 revolutions. After that it was switched to the full frequency mode and the massflow settled to 4.31 kg/s within 7 revolutions. The results were reported at last year's User's Group Conference[22]. For stall simulations, ideally all the blade passages of this compression system should be computed to adequately capture the temporal and spatial harmonics associated with stall inception. The estimated computing resources for such a full-scale calculation soon rules out all the existing platforms available for the Challenge Projects. A more conservative approach is to compute the full-annulus only in the stages where stall inception is most likely to occur, in this case the first axial stage, for low speed operating conditions. A partially full-annulus simulation was set up for this purpose. The case included full-annulus grids for the IGV and the first stage in which block-to-block interface is applied between blade passages. The remaining blade rows were modeled with only one blade passage and with phase-lag boundary conditions. This case was run at 80% design speed.

Figure 16 illustrates the domain decomposition. Each blade passage was partitioned with six blocks in the axial direction, resulting in the use of 456 blocks. This case has been test run on NAVOs SP4. It is planned to launch the simulation in the next reporting period.

4. Significance to DoD

All military and commercial gas turbine engine systems can benefit from the proposed work. In the future, this work could lead to new gas turbine engine designs with resistance to compressor stall and thus improved combat capability.

Compressors of gas turbine engines do not currently achieve their ultimate performance (pressure rise and fuel efficiency) because they must be de-rated to provide adequate margin from the compressor stall limit which, if exceeded, can lead to catastrophic engine failure. The level of de-rate, referred to as stall margin, can be as high as 35% of the total operating envelope of the compressor. Excursions towards the compressor stall limit are incurred as a result of distorted inflows encountered during military operations such as combat maneuvers and munitions release, and the stall margin is degraded over time due to erosion, rubs and normal engine wear. A 5% reduction in required stall margin will provide increased range/payload thereby significantly reducing the total logistics burden over the life cycle of the rotorcraft fleet, and could dramatically increase the vehicle operational envelope thereby enhancing combat mobility, survivability, lethality and sustainability of the objective force.

Stall control technology is applicable to all gas turbine engine powered combat and logistics support vehicles including the Comanche, Apache, Black Hawk, and Cobra rotorcraft, as well as all other manned and unmanned fixed- and rotary-wing aviation platforms, M1, and some surface ships powered by gas turbine engines. Given the pervasive applicability of this work to the vast array of gas turbine powered air and ground platforms that will comprise the objective force, operational benefits to the Army/DoD would be major, and include substantial increase in mobility, survivability, and sustainability.

5. Systems Used

ARL SP3, NAVO SP3, NAVO SP4, ARL Origin 3000

6. CTA

Computational Fluid Dynamics (CFD)

Acknowledgements

References

Suder, K.L., M.D. Hathaway, S.A. Thorp, A.J. Strazisar, and M.M. Bright, "Compressor Stability Enhancement Using Discrete Tip Injection." *ASME Journal of Turbomachinery*, Vol. 123, January 2001, pp. 14–23.

Weigl, H.J., J.D. Paduano, L.G. Frechette, A.H. Epstein, E.M. Greitzer, M.M. Bright, M.M., and A.J. Strazisar, "Active Stabilization of Rotating Stall and Surge in a Transonic Single Stage Axial Compressor." *ASME Journal of Turbomachinery*, Vol. 120, No. 4, 1998, pp. 625–636.

Spakovszky, Z.S., H.J. Weigl, J.J. Paduano, C.M. van Schalkwyk, K/L/ Suder, and M.M. Bright, "Rotating Stall Control in a High-Speed Stage with Inlet Distortion: Part I - Radial Distortion." *ASME Journal of Turbomachinery*, Vol.121, July 1999, pp.510–516.

Spakovszky, Z.S., H.J. Weigl, J.J. Paduano, C.M. van Schalkwyk, K.L. Suder, and M.M. Bright, "Rotating Stall Control in a High-Speed Stage with Inlet Distortion: Part II - Circumferential Distortion." *ASME Journal of Turbomachinery*, Vol. 121, July 1999, pp.517–524.

Strazisar, A.J., M.M. Bright, S. Thorp, D.E. Culley, and K.L. Suder, "Compressor Stall Control Through Endwall Recirculation." *ASME Paper No. GT2004-54295*, June 2004.

Skoch, G.J., "Experimental Investigation of Centrifugal Compressor Stabilization Techniques." *Journal of Turbomachinery*, October, 2003, pp. 705-713.

Hoying, D.A., C.S. Tan, H.D. Vo, and E.M. Greitzer, "Role of Blade Passage Flow Structures in Axial Compressor Rotating Stall Inception." *ASME Paper No. 98-GT-588*, June 1998.

Saxer-Felici, H.M., A. Saxer, F. Ginter, A. Inderbitzin, G. and Gyarmarthy, "Structure and Propagation of Rotating Stall in a Single Multistage Axial Compressor." *ASME Paper No. 99-GT-452*, June 1999.

Gong, Y., C.S. Tan, K.A. Gordon, and E.M. Greitzer, "A Computational Model for Short Wavelength Stall Inception and Development in Multistage Compressors." *ASME Paper No. 98-GT-476*, June 1998.

Van Zante, D.E., A.J. Strazisar, J.R. Wood, M.D. Hathaway, and T.H. Okiishi, "Recommendations for Achieving Accurate Numerical Simulation of Tip Clearance Flows in Transonic Compressor Rotors." *ASME Journal of Turbomachinery*, Vol. 122, October 2000, pp. 733–742.

Chen, Jen Ping and Jack Barter, "Comparison of Time-Accurate Calculations for the Unsteady Interaction in Turbomachinery Stage." *AIAA Paper No. AIAA-98-3293*, July 1998.

Adamczyk, J.J., "Model Equation for Simulating Flows in Multistage Turbomachinery." *ASME Paper No. 85-GT-226*, 1985.

Chen, J.P., M.L. Celestina, and J.J. Adamczyk, "A New Procedure for Simulating Unsteady Flows Through Turbomachinery Blade Passages." *ASME Paper No. 94-GT-151*, June 1994.

Shabbir, A., J. Zhu, and M. Celestina, "Assessment of Three Turbulence Models in a Compressor Rotor." *ASME Paper No. 96-GT-198*, June, 1998.

Chen, J.P. and W.R. Briley, "A Parallel Flow Solver for Unsteady Multiple Blade Row Turbomachinery Simulations." *ASME Paper No. 2001-GT-348*, June 2001.

Remotigue, M.G., "A Pre-Processing System for Structured Multi-Block Parallel Computations, Numerical Grid Generation in Computational Field Simulations." *Proceedings of the 8th International Conference*, Honolulu, HI, June 2002.

Pankajakshan, R. and W.R. Briley, "Parallel Solution of Viscous Incompressible Flow on Multi-Block Structured Grids Using MPI." In Parallel Computational Fluid Dynamics–Implementations and Results Using Parallel Computers, Edited by S. Taylor, A. Ecer, J. Periaux, and N. Satofuca, Elsevier Science, B.V., Amsterdam, 1996, pp. 601–608.

Pankajakshan, R., L.K. Taylor, M Jiang, M.G. Remotigue, W.R. Briley, and D.L. Whitfield, "Parallel Simulations for Control-Surface Induced Submarine Maneuvers." *AIAA Paper 2000-0962*, 38th Aerospace Sciences Meeting, Reno, NV, 2000.

Pankajakshan, R. and W.R. Briley, "Parallel Flow Simulations for Appended Submarines with Rotating Propulsors." *High Performance Computing: Contributions to DoD Mission Success 1998*, (DoD HPCMP), 1998, p. 61,

Reid, L., and R.D Moore, "Performance of Single-Stage Axial-Flow Transonic Compressor with Rotor and Stator Aspect Ratios of 1.19 and 1.26, Respectively, and With Design Pressure Ratio of 1.82." *Tech. Rep. TP-1338, NASA*, November 1978.

McKain, T.F. and G.J. Holbrook, "Coordinates for a High Performance 4:1 Pressure Ratio Centrifugal Compressor." *NASA Contractor Report No. 204134*, 1982.

Hathaway, M.D., J. Chen, and R. Webster, "Time Accurate Unsteady Simulations of the Stall Inception Process in the Compression System of a US Army Helicopter Gas Turbine Engine." *2003 DoD High Performance Computing Modernization Program User's Group Conference*, Bellevue, WA, June, 9–13, 2003.
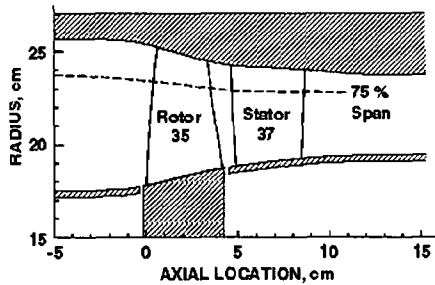
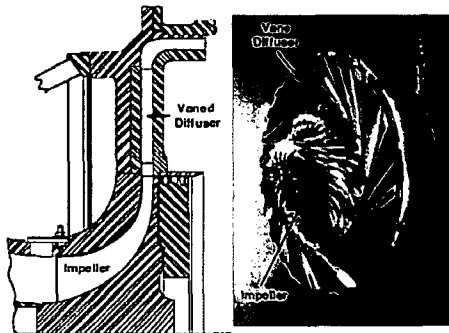Figure 1. High-speed single stage axial compressor, Stage 35, validation case

Figure 5. Comparison of TURBO predictions to experimentally measured speed lines, Stage 35

○ Solid Casing, TURBO
△ 5.9 % design flow injection, TURBO
● Solid Casing, Experiment
▲ 3.6% design flow injection, Experiment
Experiment, Weigle, 1998 ▲

Figure 2. High-speed centrifugal compressor, CC3, validation case

a) Time Traces   b) Power Spectral Density
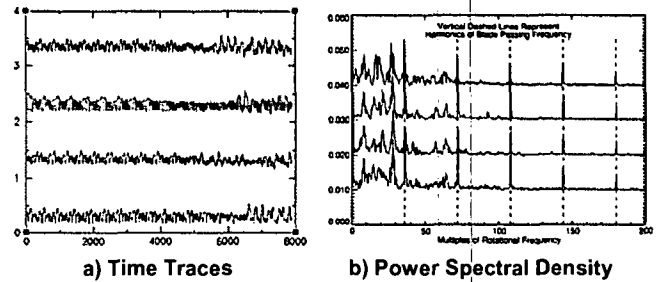
Figure 6. Axial velocity time traces and power spectral density from four equally spaced numerical probes located 10% downstream of the rotor trailing edge in the full-annulus simulations

Figure 3. Compression system of T700 engine that powers the Blackhawk helicopter

a) Iteration 6401   b) Iteration 7901
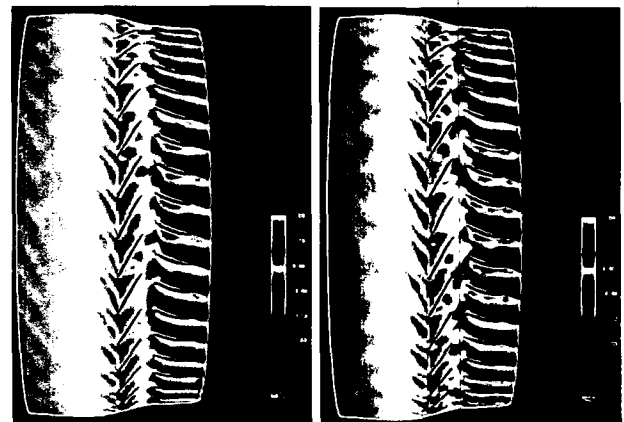
Figure 7. Axial velocity contours near the casing during stall inception at iteration 6401 and 7901, full-annulus simulation

Figure 4. Three-blade-row Grid Model for the Stage 35 simulation
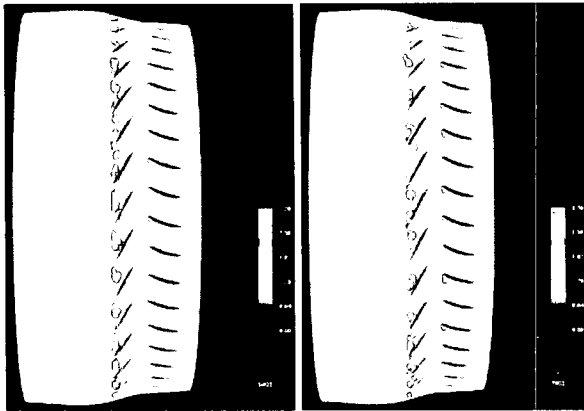
b) Iteration 7901   b) Iteration 7901

Figure 8. Entropy contours near the casing during stall inception at iteration 6401 and 7901, full-annulus simulation
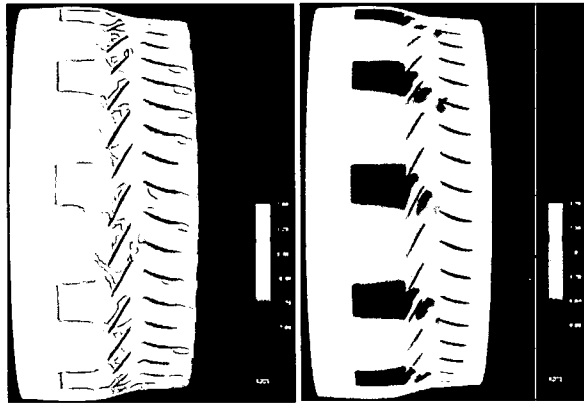
a) Axial Velocity Contours   b) Entropy Contours

Figure 9. Entropy and axial velocity contours near casing at near stall conditions, half-annulus simulation
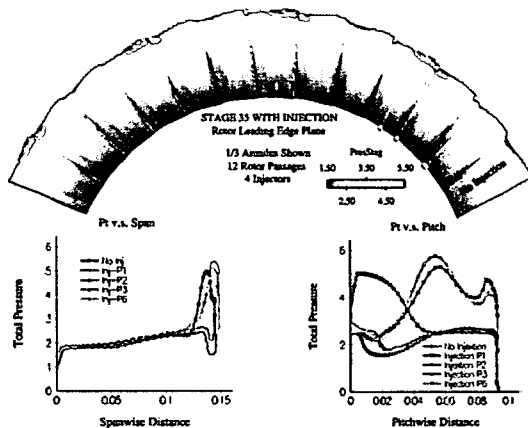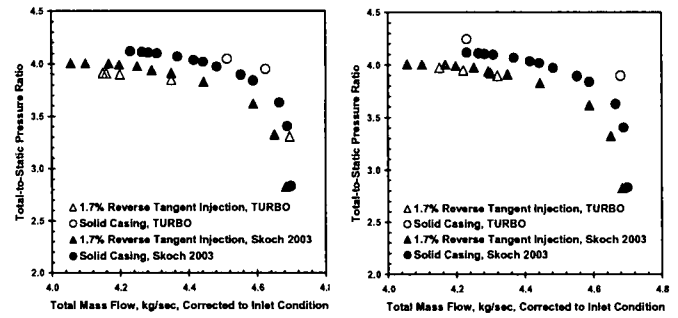

Figure 10. Full-annulus unsteady simulation of stage 35 compressor with injection showing contours of entropy which illustrate the impact of injection on the rotor flow field

a)Third-annulus simulations   b) Full-annulus simulations

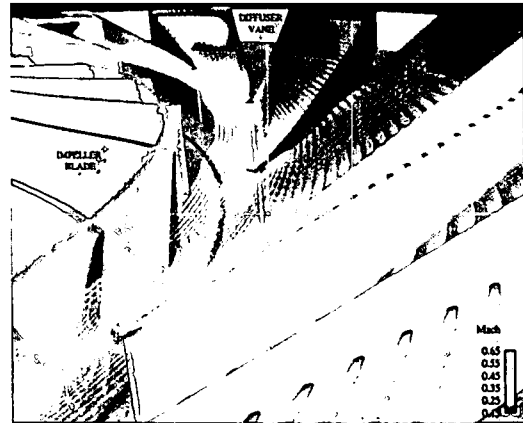**Figure 11. Comparison of TURBO predictions of CC3 to experimentally measured speed lines**

Figure 12. Near-casing velocity vectors colored by Mach number at an instant in time from results of a third-annulus simulation
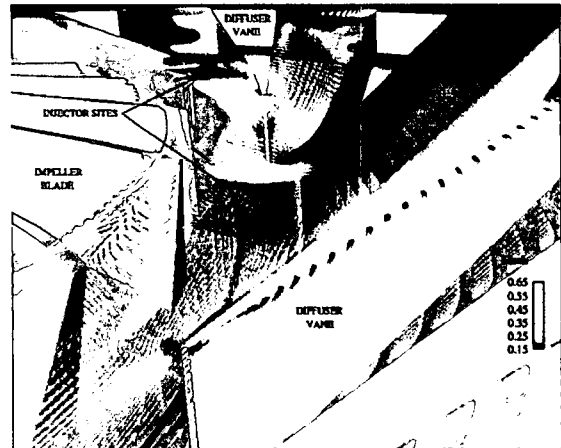

Figure 13. Near-casing velocity vectors colored by Mach number at an instant in time from results of a third-annulus with injection

TURBO SIMULATION OF CC3 CENTRIFUGAL COMPRESSOR
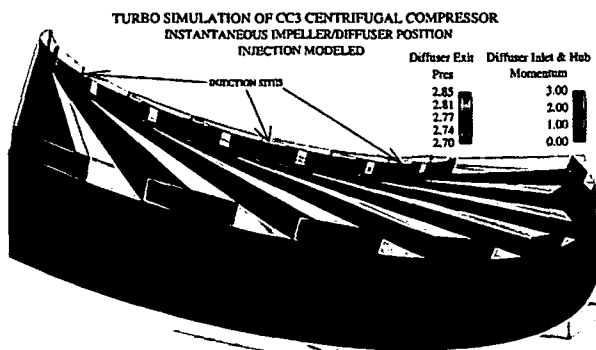INSTANTANEOUS IMPELLER/DIFFUSER POSITION
INJECTION MODELED

Figure 14 Diffuser flow field at an instant in time viewed from diffuser exit from results of a third-annulus with injection
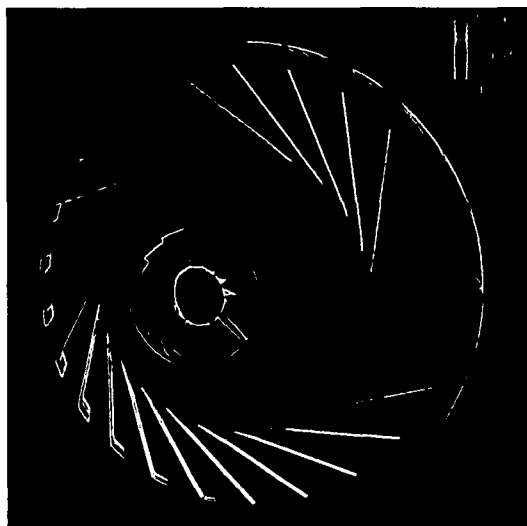

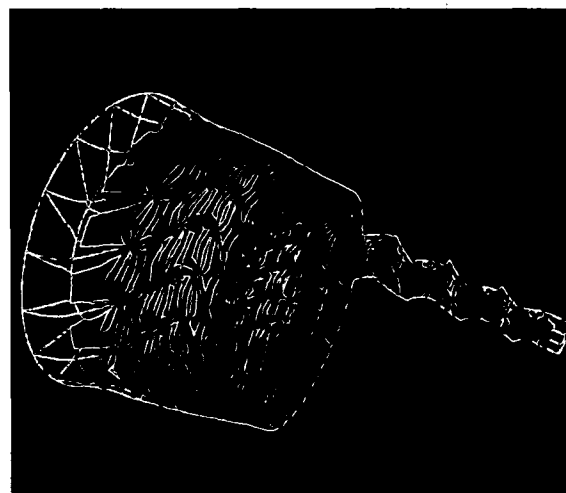Figure 15. Mach number of flow field near casing from the full-annulus simulation

Figure 16. Domain decomposition setup for a partial full-annulus simulation of the T700 multistage axial, comprises six processors per passage